FRICTION ROLLING WITH LATERAL SLIP IN RAIL VEHICLES

ROBERT KONOWROCKI
CZESŁAW BAJER

Institute of Fundamental Technological Research, Plish Academy of Sciences, Warsaw, Poland
e-mail: rkonow@ippt.gov.pl

The paper deals with the dynamic phenomena accompanying the wheel rolling over a road (rail, track), with lateral slip effects. They occur in rolling of a wheel and wheelset on a straight track in the case of lateral load and especially on curves. Different curvature radii and rotary oscillations of wheelsets result in skew rolling and, in turn, in lateral slip oscillation in the contact zone between the wheel and rail. It significantly increases noise and wear in real structures. Double periodicity of motion was detected in an underground train. Hitherto, this phenomenon has not been reported in the literature. Experimental investigation was performed on a test stand for various parameters: the angle of skew rolling, velocity and contact pressure. Results were related to a two degree-of-freedom theoretical system. In the case of steel/polyester and polyamide/polyester friction pair, qualitatively similar results were obtained.

Key words: rolling, friction, lateral slip, wheel-rail interaction

1. Introduction

Rolling contact has been investigated intensively during the last two decades (Kalker, 1990; Knothe, 1983). However, full and correct simulation of the rolling process with all phenomena that occur in the railway transport is complex. The generation of corrugations (Bajer, 1998; Hempelmann *et al.*, 1991; Kalker, 1994; Sato *et al.*, 2002) and resulting vibrations, the essential problem of rolling in railway transportation, has not been completely explained yet. Burdensome vibration transmission to the environment is in focus of researches.

Different hypotheses were assumed as a base of the analysis of wheel rolling. Some of them have minor importance and the postulated phenomena do not result in the final effect significantly, others are still being intensively

investigated. In the literature, the following cases are pointed out as a source of generation of vibrations and corrugations: imperfections in rail joints and wheel geometry (Dżuła, 1995), cone form of wheels which results in different linear speeds of the left and right wheel and snaking of trains, periodical structure of rails with sleepers and the instability of motion over periodically placed supports (Bajer and Bogacz, 2005; Bogacz *et al.*, 1995), contact problems between wheels and rails, stick and slip zones varying with a high frequency and generating waves which deform elastically or plastically both contact surfaces (Bogacz *et al.*, 1987; Brzozowski *et al.*, 1990), residual stresses caused by manufacturing and maintenance of rails and wheels (Bogacz, 1995), non-linear friction in the stick zone (Bogacz and Ryczek, 1997), influence of material hardening (Bajer, 1997), deformation of wheel/axle system as a result of impacts during rolling motion, instability of wheelset motion (Meinke and Szolc, 1996; Bogacz and Dżuła, 1993), strong hits of a perfectly round wheel rolling on an imperfect rail (Kowalska, 2008), wave phenomena in circumferential direction (Bajer, 1998), etc.

The important contribution to the problem was published by Bogacz and Dżuła (1993), Dżuła (1989, 1995). The physical continuous model was treated analytically. The wheel tire was modeled as an elastic curved Rayleigh's beam joined with the axle by means of the continuous elastic Winkler type foundation. The elastic foundation constituting the wheel disk carries out the load in three directions: circumferential, radial and perpendicular to the plane of the wheel. The curved beam theory allows one to assume the real shape of the cross-section. Frequency response functions for forced vibrations of the railway wheel prove a significant amplitude increase for the frequency 100 Hz at the velocity 200 km/h. There is no doubt that the wave propagation analysis is essential. In Bajer (1998) it was proved that steady rolling of the disc results in oscillations of contact forces. Surface waves on the circumference periodically reflect from the contact zone. The number of oscillations that suit the circumference decreases with the increase of the travelling speed while the amplitudes of contact forces increase in the same case.

In this paper, we consider a dynamic phenomenon, which occurs in rolling of the wheel over a rail with lateral slip. Such a case is involved by wind blows (both on curved and straight tracks), lateral deformation of wheels, wheelsets and rails, different linear velocity of wheels on curves and rotary oscillations of wheelsets. The skew wheel plane related to the direction of rolling results in lateral slip in the rail-wheel contact zone (Fig. 1). The rail-wheel system oscillates and generates noise. In the same time, wear considerably increases and negatively influences the environment and decreases the safety of transporta-

tion. The noise frequency is lower than in the case of corrugations generated during straight rolling, and is between 100 and 200 Hz. This low frequency noise is more burdensome for the environment and less damped than a higher frequency with an even more intensive level. Corrugations are a visible example of this oscillatory wear. However, the similar phenomenon can be observed also in rolling of a tire over a road and in the contact of rolls with a guide. In all cases, friction is the main reason of the described phenomenon. The friction law influences it qualitatively and quantitatively.
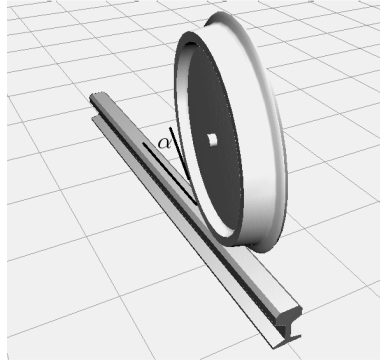

Fig. 1. Skew rolling

Kowalska in (2004, 2008) and Bogacz and Kowalska (2001) investigated the rolling over waved surfaces. Both wheel and rail irregularities were considered. The important conclusion states that short periodic irregularities of small amplitudes (0.01-0.10 mm) result in very high instantaneous normal contact forces. At a speed range of a typical train operation for low-pitch corrugations, the wheelset-rail system vibrates in the post resonance range. Amplitudes of the wheelset motion are low, while normal contact forces at corrugation peaks are significantly higher than the static load. During rolling along corrugated surfaces the high level noise is therefore generated.

Considering up-to-date publications, we can say that there are two mechanisms of wheel and rail wear. In the first one, the surface is temporarily or permanently deformed by the wave phenomenon or centrifugal forces in the domain of anisotropy involved by residual or permanent stresses. High speed rolling results in stress jumps, which in turn are sources of successive stages of periodic process. Short wave corrugations (2-8 cm) occur.

The second scenario concerns long corrugations (20-40 cm length). They appear on curves, when both wheels run over rails with different curvature. In such a case, one or both wheels roll with lateral slip. This case will be discussed

in the paper. We take here into account the elasticity of the wheelset, especially rotary flexibility of the axle and the lateral bending of the wheel disc.

Skew rolling with lateral stick and slip results in another phenomenon important in practice. Vertical stresses in contact are augmented by a significant value of residual and permanent stresses in the circumferential direction. Lateral motion in the direction of the third coordinate contributes to tangential stresses. Then the plasticity limit can be locally achieved. The oscillatory lateral motion can result in consolidation of a waved pattern.
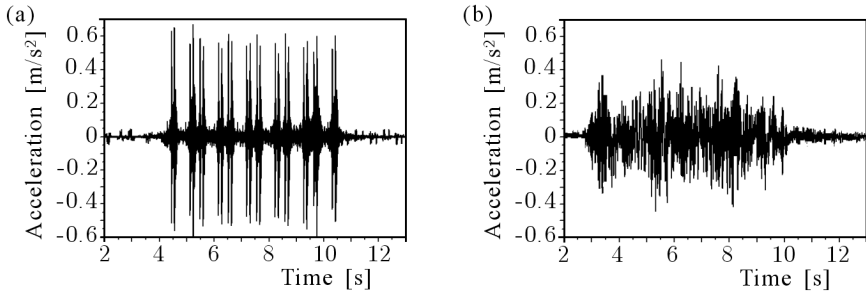

Fig. 2. Time history of vertical accelerations measured on the base of a railroad between rails on the curved section (left) and straight section (right)

Figure 2 shows vibrations measured in an underground railway tunnel. The comparison of experimental results exhibits higher amplitudes of accelerations generated on curves of the track than on its straight segments. The measurements on curves exhibited twenty four characteristic predominant groups of high amplitude vibrations. These groups correspond with the passage of successive wheelsets of bogies by the point of measurement. The effect of predominant groups of vibrations does not occur in the results registered on the straight section of the track (Fig. 2). This important feature must be emphasised here. Although vertical accelerations are three times higher than horizontal, vertical displacements are natural in the case of vertical load application. Horizontal forces are not so intuitive in rolling over a straight track. However, they propagate with significant intensity towards buildings. In Fig. 3, we show vertical displacements of the track basement. The displacements were obtained by double integration of accelerations and additional smoothing by the FFT filtering. The FFT filter smoothing stage removed components with frequencies higher than the cutoff frequency. The measurements showed that vertical displacements were about two and five times higher than lateral ones on the curved and straight sections, respectively.
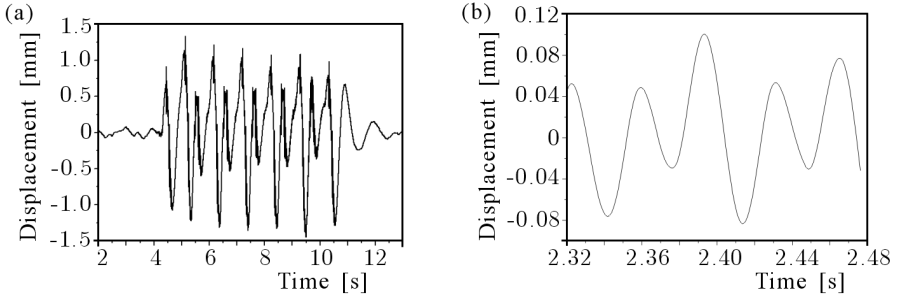
Fig. 3. Time history of vertical displacements on the curved section of the base of a railroad between rails: low frequency motion (left) and high frequency motion (right)
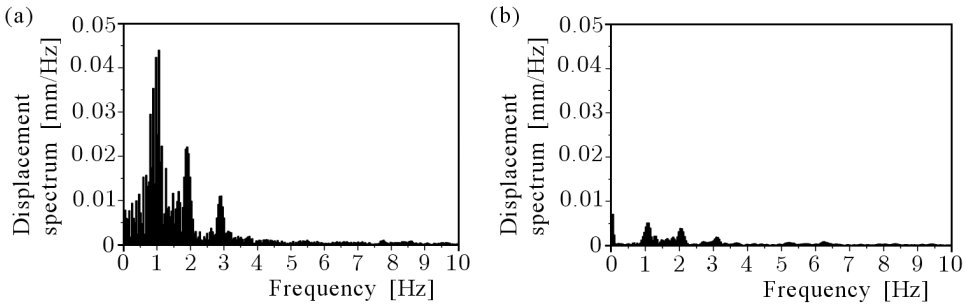

Fig. 4. Spectrum of lateral displacements on the base of the curved (left) and straight (right) section of a track

In Fig. 4, spectral analysis of experimental results of lateral displacements is depicted. Frequencies of the range 1-3 Hz on the curved segment can be noticed, whereas on the straight track the respective frequency range is equal to 1-2 Hz. The predominant frequency on the curved and straight segments of the track is equal to 1 Hz and 2 Hz. The spectral analysis showed us a double periodicity of the base motion in both cases with low contribution of the third frequency. The measurements demonstrated that lateral displacements are about 3.5 times higher on the curve than on the straight track. The double peridicity is demonstrated also in the phase plots in Fig. 5. Vibrations of the lower frequency 1-4 Hz coexist with higher frequency oscillations (15-30 Hz). The first case occurs as a result of snaking influenced by the car body motion. The second higher range frequency is caused by the low amplitude interaction of the wheel/rail system.

The first attempt to the investigation of rolling with lateral slip was made experimentally. The results of tests were compared with real vibrations of the track and the theoretical model response. Two different friction pairs were
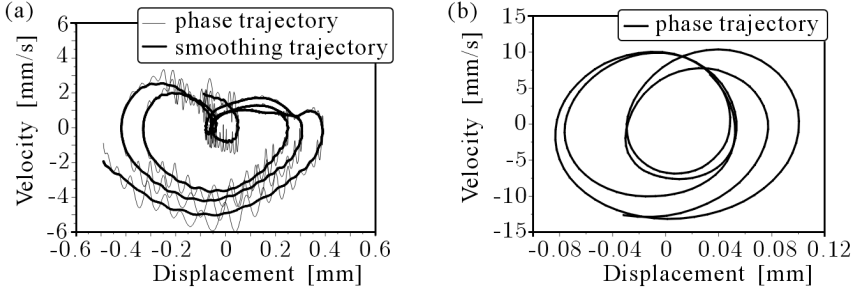
Fig. 5. Phase diagram for lateral low frequency motion 1-4 Hz of the base of the railroad on the curved section of the track (left) and the higher frequency component 15-30 Hz (right)

considered: polyester/steel and polyester/polyamide. Three different polyester belts characteristic of different surface patterns were tested, however the results did not differ qualitatively. The following parameters were examined: the speed of rolling, the angle between the wheel plane and the rolling direction (Fig. 1) and the contact force. The results strongly depended also on other parameters. In our case it was the contact time. For this reason, the experimental measurements were long lasting in order to stabilise results.

2. Experimental stand

Oscillatory lateral motion was examined in details on the experimental stand (Fig. 6). The driven belt carrier was the main part of the stand. Various belt materials were tested. Polymer and rubber surfaces were characterised by different elasticity, viscosity and friction. The tested wheels were made of steel, aluminium and polyamide. The wheel was suspended elastically on the axle by two springs that enabled its horizontal lateral motion. The springs had the longitudinal k and torsional k_φ stiffness equal to 90 N/m and 0.036 Nm/rad, respectively. They were ended by slide bearings in form of rings immersed in the grease, giving a low and constant value of the torque. The wheel was placed on the elastic belt with the adjusted contact force N.

    In the axle direction, we consider our physical model as a system of two viscoelastic spring elements that hold the wheel assumed as a lumped mass. Damping of the spring material is relatively low and can be neglected. Motion of the wheel along its axle is excited by friction. In the direction of rotation, the mass M of the inertia I_o is supported by the same set of springs with
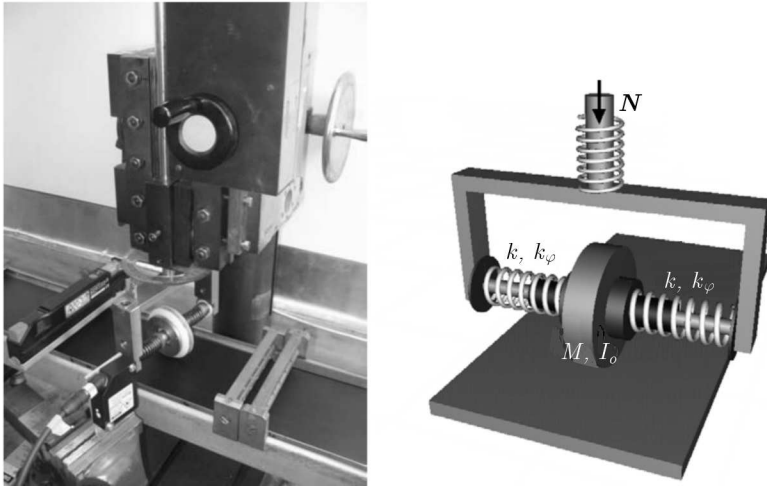
Fig. 6. Experimental stand

the stiffness k_φ. A constant low value torque (0.02-0.04 Nm) is applied to the wheel and is balanced by the spring. The wheel is subjected vertically to an external constant force N and its weight together with the suspension frame.

The friction force is equal to the force in the spring increased by a component perpendicular to the axle, induced by the slide bearings. It increases until the maximum value F_{ts}^{max} is achieved (segment 0-C in Fig. 7). We have
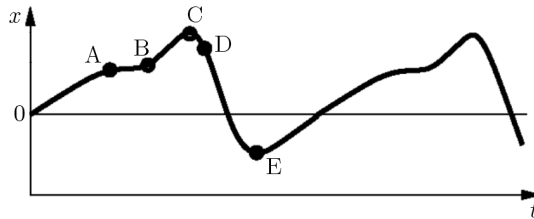

Fig. 7. Stages of the oscillation process

the stick state then. In the meantime, the stick limit is achieved (point A) by contribution of the torque. The lower kinetic friction allows motion towards the equilibrium state. Low rotary spring forces are partially released. A new stick point is established and the same process is repeated on the segment B-C. In the extremal position, the slip state starts since the friction force is lower than the elastic spring force (C-E). In the beginning of this stage (C-D), again the rotational potential energy is released. At the bottom of the diagram (po-

int E) the cycle repeats. Intermediate stages (B-C) can be placed on both the ascending and descending branch of the diagram, depending on parameters of the experiment.

Displacements in time in the wheel axle direction were registered by using laser distance transformers. They permit high resolution measurements (over 0.01 mm) and high frequency of recording (over 1000 registrations per second).

In the paper. two materials used for the wheel will be presented: steel and polyamide. The aluminium wheel was tested, however it exhibits similar properties as polyamide and will not be discussed in the paper. The diameter of the wheel was 75 mm and the width of the contact path – 9 mm.

The friction law for each tested friction pair was examined. The dependency of the friction coefficient on the relative speed was determined. The friction varied with time of sliding. We can say that the local temperature of the surface in the case of polyester increased friction in the whole speed range. Here, we do not intend to present the friction law in the test stand since both the experiment and further numerical simulations proved independency of the wheel motion of the friction function.

3.   Experimental results

The following parameters have been investigated: angle α, rolling speed v, contact pressure σ, type of friction pair. We must emphasise that all experimental results have one common feature: they exhibit double periodicity. This feature in the case of polyamide/polyester friction pair is depicted in Fig. 8.
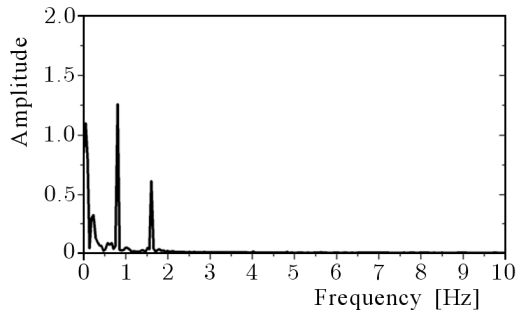

Fig. 8. Spectral analysis of the displacement function in the case of polyamide/polyester friction pair (domination of the frequencies 0.8 and 1.6 Hz)

In practice, all experimental signals for such a friction pair exhibit the same relation. Further, we shall present oscillations of the wheel in the case of two friction pairs.

In the paper, only selected and most characteristic diagrams are discussed. Other relations between the parameters will be given in conclusions.

3.1.   Polyamide/polyester friction pair

Experimental results for the polyamide/polyester friction pair for the angle $\alpha = 5°$ are depicted in Fig. 9. The most characteristic sets of diagrams were selected. Phase plots become more smooth with an increase of the rolling speed. The form of diagrams strongly depends on the vertical contact force (Fig. 10).
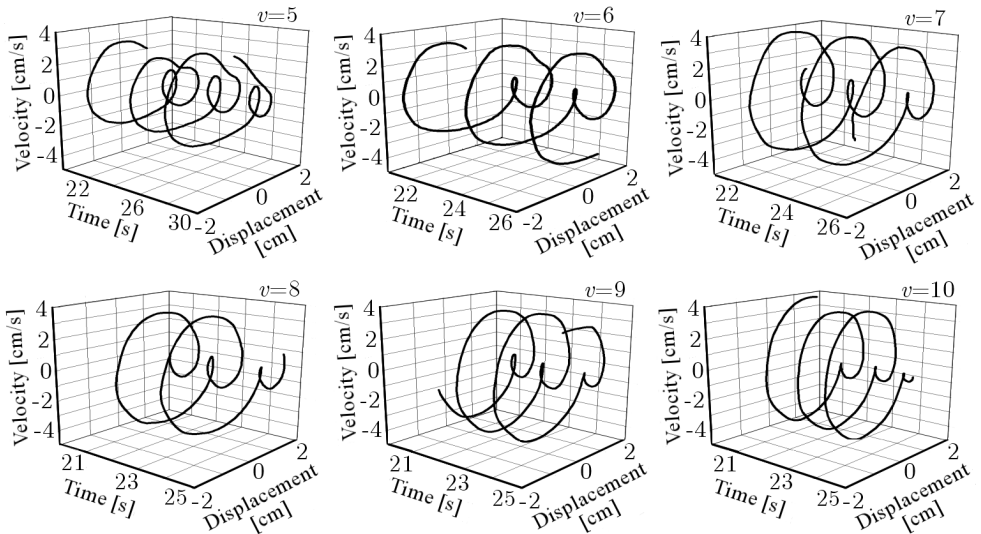

Fig. 9. Phase diagram for experimental results with the belt speed $v = 5$, 6, 7, 8, 9 and 10 cm/s (polyamide/polyester friction pair)

By changing parameters of the experiment (i.e. belt speed, angle α and mainly the contact pressure), we can obtain a phase diagram with a higher frequency loop localised in any position around the low frequency loop. In the picture low, middle and high pressure effects are depicted (3.0, 7.5 and 9.5 N of the vertical force, respectively). Other values of the pressure result in intermediate shapes.

Another interesting observation was made. The increase of the belt speed increases the amplitude of the first mode vibration and decreases the second mode amplitude. The level of the pressure force between the wheel and the
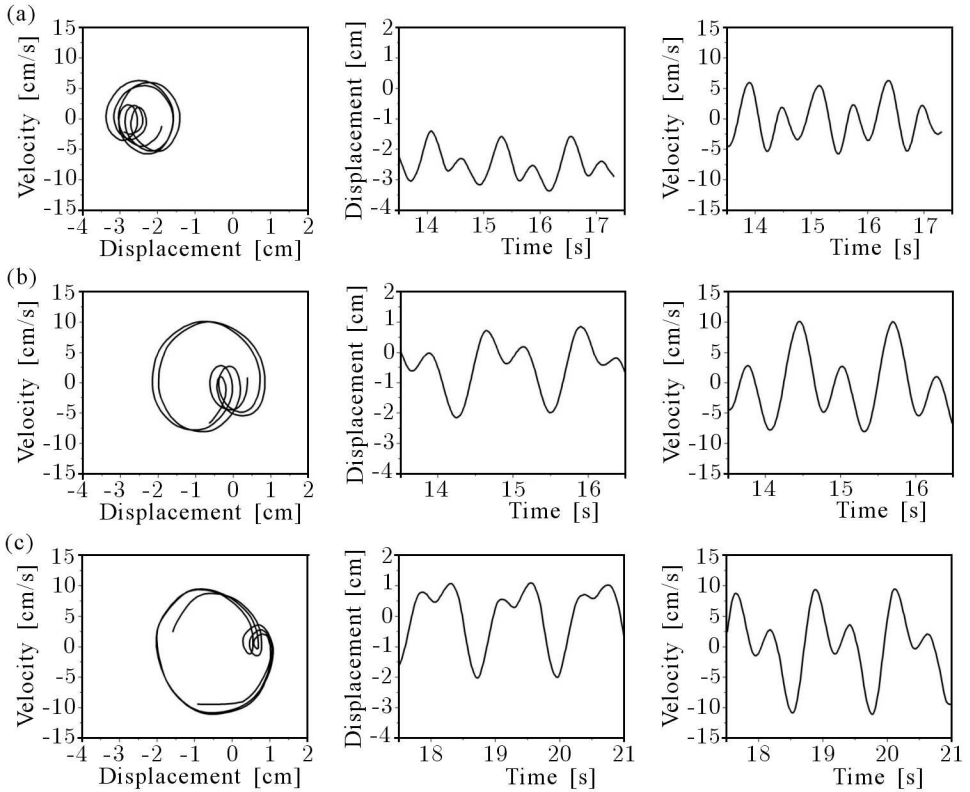
Fig. 10. Experimental phase trajectories, displacements and velocity in time for different pressure forces: (a) low, (b) middle, (c) high (for $\alpha = 5°$ and speed $v = 9\,\text{cm/s}$

belt also influences displacement diagrams. With the increase of the vertical force, we notice higher amplitudes of displacements related to the first, lower frequency mode. The second mode amplitude remains unchanged. The contact pressure alteration results in another feature. The phase shift between two modes strongly depends on it (Fig. 10). This effect is visible for small angles. When $\alpha > 10°$, the phase shift is less influenced by the pressure value.

Amplitudes depend on the belt speed but they are independent of the angle α. In Fig. 11, amplitudes vs. belt speed v are plotted for various α. All lines are almost straight in the range of investigation and coincide.

The next test with the same friction pair was performed. The polyamide wheel was loaded by two steel rings attached to its both sides. The mass of the wheel increased then by four. The final results were not affected qualitatively by the increased inertia.
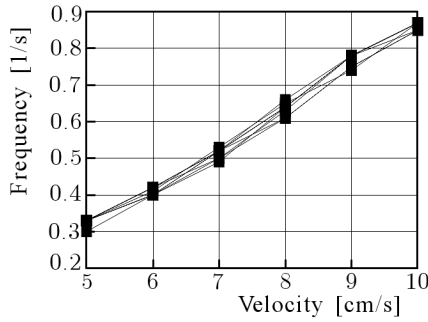
Fig. 11. Amplitudes vs. belt speed for $2° \leqslant \alpha \leqslant 10°$ (polyamide/polyester pair)

3.2. Steel/polyester friction pair

The steel wheel was manufactured as a ring (steel foot) filled inside with a polyamide thin disk. Thus the weight of the steel wheel was reduced and was comparable with the polyamide one. In this case, phase diagrams are similar to those obtained with the polyamide/polyester friction pair (Fig. 12). One can notice that the basic period is influenced by a higher order oscillation. The second and third frequency is noticed aside the main one. Mutual contribution of higher frequencies slightly varies during the experiment and in such a case the diagrams in time are less uniform than in the case of the polyamide wheel.
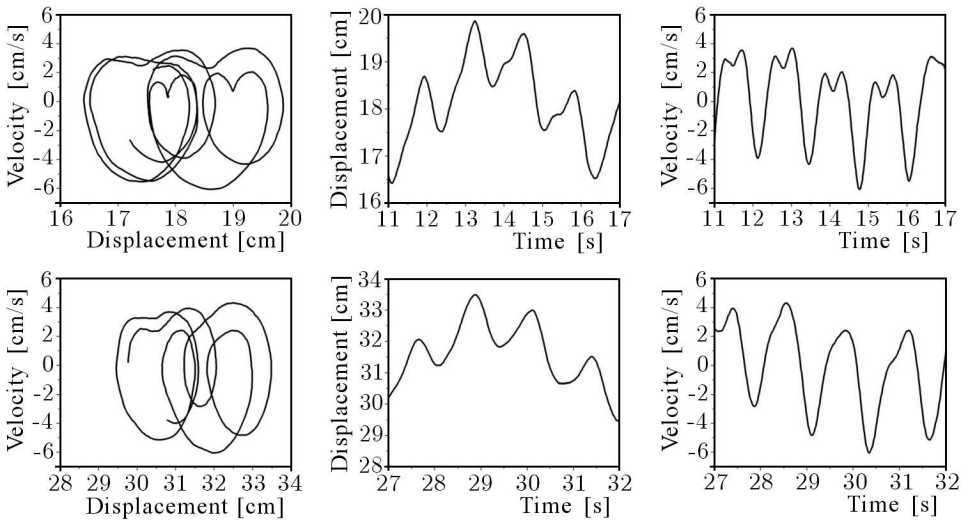

Fig. 12. Steel-polyester friction pair: phase plots, displacements and velocities for $\alpha = 10°$ (upper) and for $\alpha = 15°$ (lower) with low contact pressure

4.   Theoretical model

Experimental results exhibit double periodicity of vibrations. We propose two
a degree-of-freedom system as a mathematical model of the problem. It can
be described by the following equation

$$\begin{bmatrix} m_1 & 0 \\ 0 & m_2 \end{bmatrix} \begin{Bmatrix} \ddot{y}_1 \\ \ddot{y}_2 \end{Bmatrix} + \begin{bmatrix} f_{11}(\boldsymbol{y}, \dot{\boldsymbol{y}}) & f_{12}(\boldsymbol{y}, \dot{\boldsymbol{y}}) \\ f_{21}(\boldsymbol{y}, \dot{\boldsymbol{y}}) & f_{22}(\boldsymbol{y}, \dot{\boldsymbol{y}}) \end{bmatrix} \begin{Bmatrix} \dot{y}_1 \\ \dot{y}_2 \end{Bmatrix} + \begin{bmatrix} k_1 & 0 \\ 0 & k_2 \end{bmatrix} \begin{Bmatrix} y_1 \\ y_2 \end{Bmatrix} = \boldsymbol{0}$$

(4.1)

Two degrees of freedom correspond to the lateral and rotary motion of the
wheel, respectively. Both inertia and stiffness matrices are constant. The damp-
ing coefficients depend on velocities and displacements of both degrees of
freedom. We have a parametric excitation in a general case. Below we shall
establish the functions f_{ij} to fit the experimental results.

The friction influence is the fundamental question in our problem. It affects
the higher frequency vibration. We assume it as a nonlinear one depending
on the relative velocity of the belt and wheel and the position of the wheel.
We neglect the dependency of friction on the adhesion time and the force
rate (Bogacz and Ryczek, 1997). The periodic motion depends on the belt
velocity v, angle α and, mainly, physical (frictional) properties of the friction
pair (wheel-belt). We simplify our theoretical model. The wheel is assumed to
be a rigid body, the springs exhibit linear elasticity (axial and rotational) and
negligible internal viscous damping, and the belt is indeformable in the plane.
Its moving velocity is constant.

The principal mode of vibrations is related to lateral motion of the wheel
and the higher mode – to the rotary motion. In our discrete model (4.1), these
both degrees of freedom are denoted by y_1 and y_2.

4.1.   Polyamide/polyester friction pair

Below we present our experimental results registered for the polyami-
de/polyester friction pair in comparison with theoretical functions. We must
emphasise that diagrams obtained experimentally were repeatable with good
accuracy. Double periodicity was observed in all cases. The following equation
generally describes the wheel motion

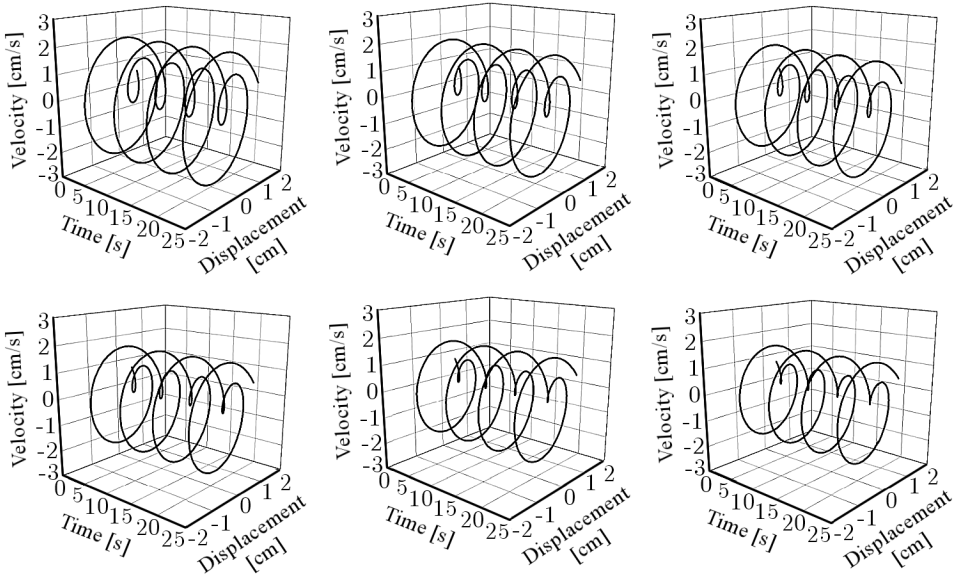$$x = \sin t + a \sin(2t + b) \qquad\qquad v = \cos t + 2a \cos(2t + b) \qquad (4.2)$$

Fig. 13. Theoretical phase plots for parameters a and b collected in Table 1

Table 1. Parameters a and b for different belt speed

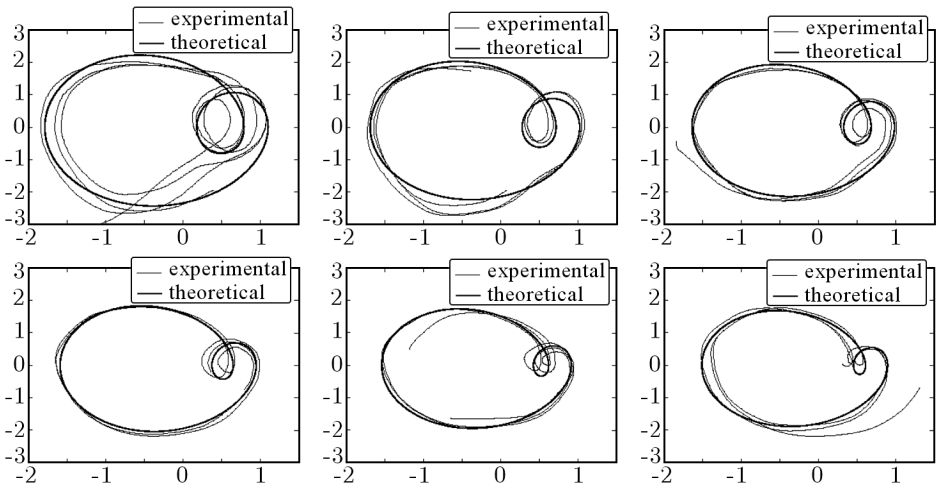| v [cm/s]	5	6	7	8	9	10
a	0.80	0.70	0.65	0.60	0.55	0.52
b	1.90	1.90	1.90	1.90	1.90	1.90

Fig. 14. Theoretical and experimental phase trajectories (u – speed, x – displacement, angle $\alpha = 5°$ and belt speed $v = 5\text{-}10\,\text{cm/s}$)

Phase diagrams allowed us to select characteristic features of motion for various rolling parameters (Fig. 14). For various belt speeds from the range $v = 5\text{-}10\,\text{cm/s}$, the parameters a and b have values presented in Table 1 and plotted in Fig. 15.
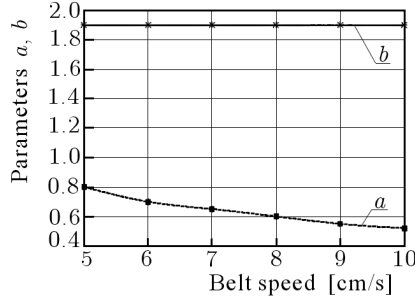
Fig. 15. Dependency of the parameters a and b on the belt speed

f_{12} is a linear combination of the velocity and displacement of the second degree of freedom. Unilateral coupling of both equations must be pointed out. In such a case, the second degree of freedom serves as a source of a harmonic signal for the first degree of freedom. In practice both ways of coupling exist, however, with minor influence of the way opposite to the dominating one.

For example, we can obtain phase plots identical as in Fig. 10 – the first one for the initial conditions: $q_1 = q_2 = 0$, $v_1 = -0.1$, $v_2 = 1$, and excitation $F_1 = 0.2v_2 + 0.15q_2$, the second one for $q_1 = q_2 = 0$, $v_1 = -0.1$, $v_2 = 1$, $F_1 = -0.2v_2 + 0.20q_2$, and the third one for $q_1 = q_2 = 0$, $v_1 = 0.1$, $v_2 = -1$, $F_1 = 0.2v_2 + 0.15q_2$.

4.2. Steel/polyester friction pair

The discrete system is composed of two degrees of freedom, as in the previous case. A proper selection of functions f_{ij} allows us to obtain numerical results coinciding the experimental ones. One can select several pairs of parameters a, b and initial conditions that give simulation results coinciding with the experiment. We propose the following initial conditions: $q_1 = q_2 = 0$, $\dot{q}_1 = -0.2$, $\dot{q}_2 = 1.0$. The coincidence with experiments is achieved for $f_{11} = f_{21} = f_{22} = 0$ and f_{12} as a function of the velocity and the displacement

$$f_{12} = c_1(|v_2| + c_2)^2 + c_3q_2 \tag{4.3}$$

As an example we consider $m_{11} = 16$, $m_{22} = 1$, $k_{11} = k_{22} = 1$ and $c_1 = 24$, $c_2 = -0.5$, $c_3 = -18$ in function (4.3). The velocity v_2 contributes to the

friction term. The displacement q_2 shifts the second branch on the diagram (Fig. 16d). f_{12} introduces a parametric excitation (compare with Fig. 12). The
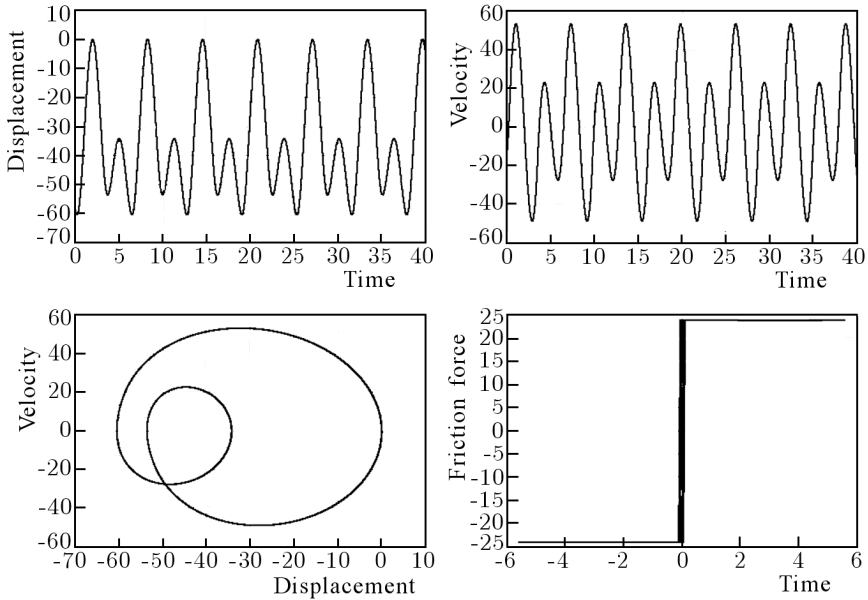

Fig. 16. Displacement in time, velocity in time, phase plane and friction coefficient ($m_1/m_2 = 1$ and parameters $p_1 = 0$, $p_2 = 0$, $p_3 = 24$, $v_1 = 3.00$ and $v_2 = 5.6$)

analytical function which describes lateral motion of the steel wheel can be written as

$$y = -\sin t + a\sin(2t) + b\sin\frac{t}{4}$$

$$\dot{y} = -\cos t + 2a\cos(2t) + \frac{b}{4}\cos\frac{t}{4}$$

(4.4)

We can notice that the multiplier of the second frequency is four instead of two as in the case of the polyamide wheel. We can explain this as the influence of the U-shaped friction function for the steel/polyester pair.

Let us compare the experimental results (Fig. 12) with analytical plots of functions (4.4) (Fig. 17). Both results in Fig. 17 correspond to the low contact pressure case at angle 10° and 15°. They are plotted for $a = -0.35$, $b = 1.4$ and $a = -0.15$, $b = 1.4$ (Eqs. (4.4)), respectively. One can notice that the third term in (4.4) with the scaling coefficient b produces long period oscillations (four times longer comparing with the base period, see for example Fig. 16b,c).

Characteristic oscillations for the steel wheel are generated by the first two terms and are qualitatively identical as in the case of the polyamide wheel.
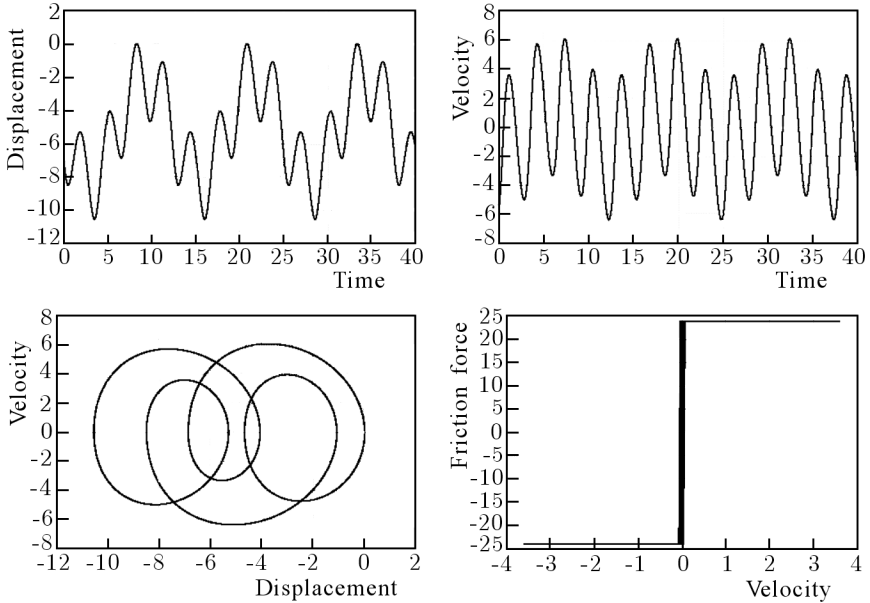

Fig. 17. Displacement in time, velocity in time, phase plane and friction coefficient ($m_1/m_2 = 4$ and parameters $p_1 = 0$, $p_2 = 0$, $p_3 = 24$, $v_1 = 0.70$ and $v_2 = 3.6$)

5.   Conclusions

Experimental investigations of the problem of skew rolling allowed us to prove double periodicity of lateral motion of the wheel. In the case of strongly non-linear friction law (steel), the third frequency of minor contribution is observed. This frequency is double according to the fundamental period.

First of all, the frequencies of oscillations do not depend on the angle α while the amplitudes increase with the increase of this angle. In the case of small angles α, the phase shift of two modes strongly depends on the contact pressure. For higher values of N this dependency is not so direct. Stick-slip type of vibrations can be noticed for small N. For higher values, the stick phase disappears. Further research will enable us to define the mechanical system which produces displacement/velocity time characteristics identical with the experimental ones. A single degree of freedom system with a strongly non-linear

friction law applied to the vibrating mass does not allow obtaining satisfactory results, since it requires a harmonic excitation. In our experiment, the rotary degree of freedom supplies this mode. That is why the two degree-of-freedom system seems to be appropriate to result in double periodic vibrations. This also concerns the rolling of the steel wheel which exhibits an increase of the friction coefficient with the velocity. Theoretical results coincide with the response of our physical model with the first degree of freedom related to lateral motion of the wheel and the second one corresponding to wheel rotations. A soft coupling is promising in investigation of the self-excited response.

Intuitively, we expect faster lateral motion and spring compression in the case of higher angles. Thus, one oscillation could be performed in a shorter time. The experiment proves the independency of the main frequency of the angle. In turn, the angle influences the amplitude level.

The experimental investigation will be continued for other friction pairs. The dependence of the friction coefficient on the rolling speed, the angle and contact pressure in a full form will be established. The experiment preformed in a real scale should be the final stage of the research.

References

1. BAJER C., 1997, Numerical space-time modelling of dynamic contact problems, *IFTR Reports*, Warsaw, **5** [in Polish]

2. BAJER C.I., 1998, The space-time approach to rail/wheel contact and corrugations problem, *Comp. Ass. Mech. Eng. Sci.*, **5**, 2, 267-283

3. BAJER C., BOGACZ R., 2005, Propagation of perturbances generated in classic track, and track with Y-type sleepers, *Arch. Appl. Mech.*, **74**, 754-761

4. BOGACZ R., 1995, Residual stresses in high-speed wheel/rail system; Shakedown and corrugations, In: *Proc. of the 1-st European Conference on Steel Structures EUROSTEEL'95*, A.N. Koanadis (Edit.), Athens, A.A. Balkema, 331-343

5. BOGACZ R., BRZOZOWSKI M., MAHRENHOLTZ O., ROŃDA J., 1987, Dynamic effects in a rolling contact problem, *ZAMM*, **67**, 4, T176-T179

6. BOGACZ R., DŻUŁA S., 1993, Dynamics and stability of a wheelset in rolling contact motion on rails, *Proc. of ITTG International Symposium on the Technological Innovation in Guided Transports*, Lille, France, 871-883

7. BOGACZ R., KOWALSKA Z., 2001, Computer simulation of the interaction between a wheel and a corrugated rail, *Eur. J. Mech A/Solids*, **20**, 637-684

8. Bogacz R., Krzyżyński T., Popp K., 1995, Application of floquet's theorem high-speed train/track dynamics, In: *Advanced Automotive Technologies, ASME Congress*, 55-61

9. Bogacz R., Ryczek B., 1997, Dry friction self-excited vibrations analysis and experoment, *Eng. Transactions*, **45**, 3/4, 487-504

10. Brzozowski M., Bogacz R., Popp K., 1990, Zur reibungsmodellierung beim rollkontakt (on the modelling of wear in rolling contact), *ZAMM*, T678-T680

11. Dżuła S., 1989, Free vibration of wheelset wheel, *Arch. Mech. Engng.*, 2/3, 97-124

12. Dżuła S., 1995, Forced vibrations of the rotating railway wheel, *Cracow Univ. of Technology, Selected Problems*, **3**, 307-323

13. Hempelmann K., Hiss F., Knothe K., Ripke B., 1991, The formation of wear patterns on rail tread, *Wear*, 179-195

14. Kalker J.J., 1990, *Three-Dimensional Elastic Bodies in Rolling Contact*, Kluwer Academic Pablisbers

15. Kalker J.J., 1994, Considerations on rail corrugation, *Vehicle System Dynamics*, **23**, 3-28

16. Knothe K., 1983, *Rail Corrugations*, ILR Bericht 56, Berlin

17. Kowalska Z., 2004, Vibro-impact motion of heavily loaded compact hard bodies, *Engng. Trans.*, **52**, 1/2, 37-55

18. Kowalska Z., 2008, Vibro-impacts induced by irregular rolling surfaces of railway rails and wheels, *J. Theor. Appl. Mech.*, **46**, 1, 205-221

19. Meinke P., Szolc T., 1996, On discrete-continuous modelling in the railway wheelsets for non-linear dynamic analysis in the medium frequency range, *Proc. 2 Europ. Nonlinear Oscillation Conf., Euromech*, Praque, 135-138

20. Sato Y., Matsumoto A., Knothe K., 2002, Review on rail corrugation studies, *Wear*, **253**, 1/2, 130-139

Tarcie toczne z poślizgiem bocznym w pojazdach szynowych

Streszczenie

W pracy omówiono zjawiska dynamiczne związane z toczniem się koła z poślizgiem bocznym po drodze (szynie, torze). Mają one miejsce przy toczeniu się kół lub zestawów kołowych po torze prostym, w przypadku bocznego obciążenia oraz na łukach. Różne promienie krzywizn oraz drgania skrętne zestawów kołowych powodują ukośne

toczenie i boczne poślizgi w strefie kontaktu koła z szyną. Zjawisko to znacząco zwiększa hałas oraz zużycie elementów konstrukcji. W kolei podziemnej wykryto dwuokresowość drgań. Zjawisko to dotąd nie było opisywane w literaturze. Przeprowadzono stanowiskowe badania eksperymantalne z uwzględnieniem następujących parametrów: kąta ukośnego toczenia, prędkości oraz siły nacisku w strefie kontaktu. Wyniki odniesiono do ruchu teoretycznego układu o dwóch stopniach swobody. W przypadku par ciernych stal-poliester i poliamid-poliester uzyskano zbliżone jakościowo rezultaty.